JOURNAL OF CATALYSIS 113, 367–382 (1988)

Selective Synthesis of Dimethylamine over Small-Pore Zeolites

I. H–RHO

R. D. SHANNON, M. KEANE, JR., L. ABRAMS, R. H. STALEY, T. E. GIER, D. R. CORBIN, AND G. C. SONNICHSEN

E. I. du Pont de Nemours & Company,[1] Central Research and Development Department, Experimental Station, Wilmington, Delaware 19898

Received August 26, 1987; revised May 16, 1988

Zeolite H–RHO is highly selective for the synthesis of dimethylamine (DMA) from methanol and ammonia. Shallow-bed *dry* calcination of NH_4–RHO at temperatures from 400 to 700°C results in progressive deammoniation, dehydroxylation, and dealumination and in dimethylamine (DMA) and trimethylamine (TMA) selectivities that progressively change from 50 to 67% and 25 to 5%, respectively. Concurrent changes in dealumination and internal and external acid sites suggest a process whereby DMA selectivity arises from destruction of nonselective sites on impurity phases such as pollucite and/or from hindered TMA diffusivity by either nonframework Al species (NFA) or NFA/methylamine adsorption complexes. Shallow-bed *steam* calcination at temperatures from 400 to 700°C results in higher degrees of dehydroxylation and dealumination than shallow-bed *dry* calcination and in DMA and TMA selectivities that change from 50 to 71% and 20 to 2%, respectively. The higher DMA selectivities result from the higher degree of dealumination and/or the more effective deactivation of impurity phases. Increased activity of shallow-bed steamed H–RHO is correlated with destruction of most of the highly acidic 3610 cm^{-1} Brønsted sites and to their replacement with weakly acidic 3640 cm^{-1} OH groups. High dimethyl ether yields observed in samples calcined above ~650°C are associated with an OH band at 3680 cm^{-1} and attributed to the condensation of nonframework Al species.

INTRODUCTION

It was recently shown that the zeolites H–RHO, H–ZK-5, and chabazite are highly selective and active catalysts for the synthesis of dimethylamine (DMA) from the reaction of methanol and ammonia (*1–3*). Lower selectivities or activities have been found for other zeolite catalysts such as erionite, chabazite–erionite, 5A, Fu-1, Nu-3, and mordenite at reaction temperatures of 300–325°C (*4–11*).

H–RHO and H–ZK-5 are unusual in that they provide DMA selectivities of 50 to 70% at operating temperatures of 325°C and can provide DMA and TMA (trimethylamine) selectivities similar to those of the commercial methylamine demand (*1*). The DMA and TMA selectivities over H–RHO depend strongly on the method and temperature of calcination of the NH_4–RHO precursor. This paper describes the physical and catalytic properties of RHO catalysts prepared by various calcination techniques.

EXPERIMENTAL

Sample, Na,Cs–RHO "A," was prepared by adding a mixture of 200 ml 4 *M* Na_2AlO_2OH, 56 ml 50% CsOH, and 26 g NaOH to 720 ml of colloidal silica (Ludox LS-30) in a polytetrafluoroethylene (Teflon) bottle and allowing it to stand at 25°C for 9 days. The resulting mixture was heated at 100°C for 7 days, cooled and maintained at 25°C for an additional 3 days, and then reheated to 100°C for 24 h. After three 16-h exchanges at room temperature in 20% aq NH_4NO_3, wet chemical analysis of the resultant NH_4–RHO indicated the composition $(NH_4)_{9.6}Cs_{1.1}Al_{10.3}Si_{37.7}O_{96} \cdot 42.9H_2O$.

[1] Contribution No. 4472.

0021-9517/88 $3.00

Two additional samples of Na,Cs–RHO were prepared according to the method just described. Both samples were maintained at 25°C for 6 days and then heated to 92–98°C for 4 and 6 days, respectively. These samples were combined, labeled Na,Cs–RHO "B," and exchanged four times at 80°C with 10% aq NH_4NO_3 to yield $(NH_4)_xCs_{0.70}Al_{10.6}Si_{37.4}O_{96} \cdot xH_2O$.

γ-Al_2O_3 was prepared by calcination of AlOOH (Catapal-SB) at 500°C for 15 h.

Three separate procedures were used to calcine the samples: dry shallow-bed (SBN), shallow-bed steam (SBST), and deep-bed (DB). Dry shallow-bed calcination consisted of moving a 5- to 10-g sample, in a quartz boat of 100 cm^2 area, through the hot zone of a belt furnace for 4 h. Rapid removal of H_2O and NH_3 was assured by a 20 liter/min flow of N_2 over the sample.

Shallow-bed steaming was carried out by heating NH_4–RHO in a quartz boat for 1 h under rapidly flowing N_2 (1 liter/min) to produce H–RHO and then maintaining the sample at temperature for 4 h under 1 liter/min N_2 equilibrated with water to provide the desired H_2O partial pressure.

Deep-bed calcination was carried out for 4 h at 650°C using a 5-g sample placed in a covered crucible of 2.5 cm diameter and 5.0 cm height.

Samples are designated using the terminology of Fischer *et al.* (*12*) where S refers to SBN calcination and SS to SBST calcination, followed by the calcination temperature in degrees Kelvin.

In order to determine the reproducibility of the SBN and SBST processes, five samples of Na,Cs–RHO were made by techniques essentially identical to those of sample A and after exchange with NH_4NO_3 solutions to yield 0.25–1.0 Cs/uc, were calcined by the SBN and SBST processes described above.

X-ray diffraction patterns were obtained on a Phillips APD 3600 diffractometer. Typical patterns for SBN and SBST samples are shown in Fig. 1. X-ray crystallinity was estimated from the intensity of the RHO (420) peak at 2θ (Cu$K\alpha$) = 26.6°. Infrared experiments were performed according to the procedure previously described (*12, 13*). Internal Lewis site concentration was estimated from adsorption of MeCN and measurement of the CN stretching peak at 2330 cm^{-1}. External Lewis and Brønsted concentrations were obtained by adsorption of pyridine and measurement of intensities at 1455 and 1545 cm^{-1}, respectively.

Adsorption experiments were carried out as described earlier (*12*). In addition, TMA sorption experiments were performed over the temperature range 50 to 300°C.

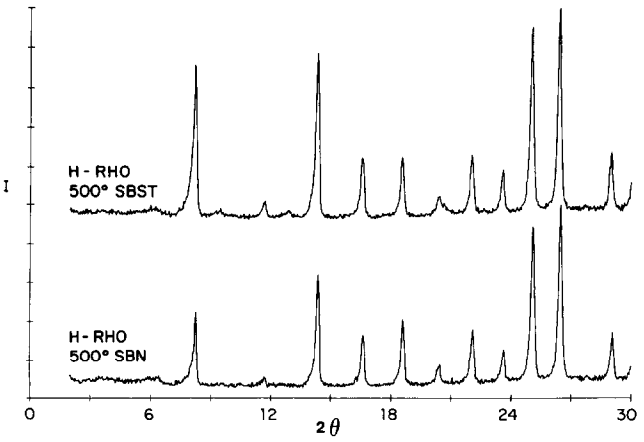

FIG. 1. X-ray diffraction patterns of shallow-bed and steamed H–RHO zeolites. Cu$K\alpha$ radiation.

To evaluate catalytic behavior, the catalysts were pelletized and then crushed to pass through −20/+40 U.S. Standard testing sieves. A 1.0- to 2.0-g catalyst charge was placed in a 0.635-cm-diameter, 304 stainless-steel U-tube reactor. A methanol : ammonia mixture at a molar ratio of 1 : 1 was fed as a vapor over the catalyst at 250–400°C and 1 atm. Molar concentrations of products and reactants in the reactor effluent were measured by gas chromatography (GC). Errors associated with the GC traces were about ±3% of the reported values. Feed rate and reactor temperature were varied to obtain as wide a range of reactant conversion as possible. Multiple data were obtained under each condition to ensure stable reactor operation; i.e., the reactor was lined out and the catalyst showed constant activity. No catalyst deactivation was observed over normal runs of ~8 h. Chromatograms were stored in a computer database.

Data were fit to a second-order reaction mechanism

Series-Parallel

$$NH_3 + MeOH \xrightarrow{k_1} MMA + H_2O \quad (1)$$

$$MMA + MeOH \xrightarrow{k_2} DMA + H_2O \quad (2)$$

$$DMA + MeOH \xrightarrow{k_3} TMA + H_2O \quad (3)$$

Disproportionation

$$MMA + MMA \xrightarrow{k_4} DMA + NH_3 \quad (4)$$

$$DMA + DMA \xrightarrow{k_5} TMA + MMA \quad (5)$$

Side-Parallel

$$2\ MeOH \xrightarrow{k_6} DME + H_2O \quad (6)$$

Kinetic analyses were performed with the Gear integration program, HAVCHEM (*14*), to give rate constants, relative to the first step by setting $k_1 = 1$.

A typical fit of the mechanism to chromatographic data was given for H–RHO in Keane *et al.* (*1*). The primary relative rate constants of interest are DMA formation, k_2, and TMA formation, k_3. The ratio, k_2/k_3, is a measure of DMA selectivity which is independent of initial feed composition, catalyst activity, and extent of reaction. In general k_2 remains relatively constant over H–RHO and increases in k_2/k_3 result from decreases in k_3. Values of $k_2/k_3 > 1$ indicate selectivity to DMA vs TMA whereas $k_2/k_3 < 1$ indicate a product distribution closer to the equilibrium value.

In addition to the rate constants, molar selectivities of DMA and TMA are reported at 90% MeOH conversion. For example, DMA molar selectivity is calculated as

$$\%\ \text{DMA} = \frac{\text{mol DMA}}{\text{mol MMA} + \text{mol DMA} + \text{mol TMA}} * 100\%.$$

By-product dimethyl ether, DME, yield is calculated as

$$\%\ \text{DME} = \frac{\text{mol DME} \times 2\ \text{mol MeOH/mol DME}}{\text{mol MeOH converted}} * 100\%.$$

MeOH conversion at 90% was chosen to report DMA and TMA selectivity, and DME yield, since this represents a commercially practiced reactant conversion, and amine selectivities vary considerably with conversion.

Space velocity, which correlates to catalyst activity, was obtained from the reactant feed rates and catalyst charge. Space velocity data under typical reactor conditions of 90% MeOH conversion, 325°C, 1 : 1 NH_3 : MeOH feed composition, and 1 atm were used to compare catalyst activities. This basis demonstrates utility in the range of commercially practiced MeOH conversions and feed compositions and represents the typical operating temperature for H–RHO.

RESULTS

A. NH_4–RHO Precursor

Na,Cs–RHO can contain a variety of im-

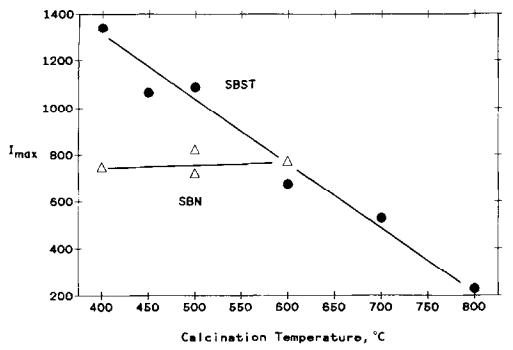

FIG. 2. Intensity of RHO 420 peak (Cu$K\alpha$) vs calcination temperature for SBN and SBST samples.

purities—gel, chabazite, P_c, pollucite, and several phases of unknown structure. Gel is present if the RHO crystallization is stopped prematurely. Chabazite, in the form of spherical aggregates, is always present at 5–10% levels. P_c (*15–17*) appears irregularly at low levels, whereas a pollucite phase, believed to be similar to $CsAlSi_2O_6 \cdot nH_2O$ appears at the later stages of crystallization and increases as the crystallization is carried out for longer periods. In samples A and B, only chabazite was detected by X-ray diffraction; however, the presence of small amounts of P_c and pollucite below the limits of detection by X-ray diffraction cannot be ruled out. NH_4^+ exchange is expected to produce a mixture of NH_4–RHO and NH_4–chabazite. A more detailed analysis of the impurity phases and their effects on the behavior of H–RHO catalysts in DMA synthesis will be given in the second paper of this series.

B. Shallow-Bed Calcination

Heating NH_4–RHO at increasing calcination temperatures, T_c, from 400 to 600°C in rapidly flowing N_2 yields H–RHO products with very little change in crystallinity (see Fig. 2). Calcination in the lower temperature range, from 400 to 500°, must be carried out for longer periods to obtain H–RHO free of NH_4^+ as indicated by IR. For example, 31 h is necessary to remove NH_3 at 400°C whereas only 4 h is sufficient at 600°C.

SBN calcination at 500 or 600°C results in slight dealumination of H–RHO as evidenced by a midinfrared spectrum where ν(TO) increased to 1060 cm^{-1} from 1053 cm^{-1} for NH_4–RHO. As T_c increases from 400 to 600°C, ν(TO) increases gradually to 1064 cm^{-1}, and then to 1073 cm^{-1} as T_c reaches 700°C (see Fig. 3). The framework composition after calcination at 600°C corresponds approximately to $H_{8.3}Cs_{0.7}Al_9Si_{39}O_{96}$ (*18*).

Samples calcined at 500–600°C display a band at 3610 cm^{-1} attributed to highly acidic bridging OH groups (Shannon *et al.*, *13*). As T_c is increased from 500 to 700°C, the intensity of the 3610 cm^{-1} band decreases and a shoulder at 3640 cm^{-1} appears.

Catalytic data for SBN-calcined H–RHO are summarized in Table 1. DMA selectivity increases from ~50% (k_2/k_3 = 3.7) for H–RHO-S673 to ~70% (k_2/k_3 = 17) for H–RHO-S873. Figure 4 shows a gradual increase in DMA selectivity (k_2/k_3) with T_c up to 600°C and a slight decrease at 700°C. The sample calcined at 700°C has a considerably reduced MeOH sorption value of 13.2% compared to samples calcined at lower temperatures (Table 1).

At temperatures less than 125°C, TMA sorption was ≤1%, the amount corresponding to the coverage on the external surface. Above 150°C, TMA readily sorbs into the

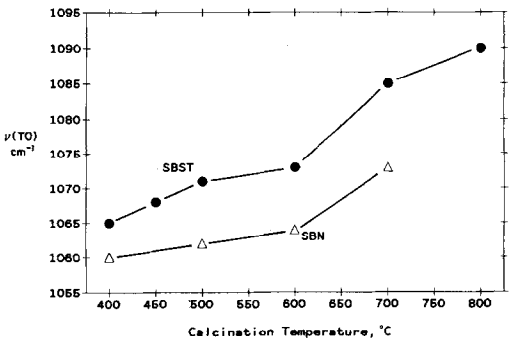

FIG. 3. TO stretching frequency (ν(TO)) vs calcination temperature of shallow-bed and steamed H–RHO.

TABLE 1

Effects of Calcination Temperature on Properties of Dry Shallow-Bed Calcined H–RHO A (1.0 Cs/uc)

T (°C)	Atm	Hour	ν(TO) (cm^{-1})	a (Å)	SV (h^{-1})	DME (%)	DMA (%)	TMA (%)	k_2/k_3	k_2	k_3	I_{max} (cps)	MeOH (%)	I(OH) (3740 cm^{-1})	I(OH) (3610 cm^{-1})	I(OH) (3640 cm^{-1})	I(OH) (3680 cm^{-1})	I(MeCN) (2330 cm^{-1})	I(PyrB) (1545 cm^{-1})	I(PyrL) (1455 cm^{-1})
400	N_2	31	1060	14.98	1.8	5	52	21	3.67	4.8	1.30	750	21.4					0.087		
500	N_2	4	1060	14.97	1.3	5	49	25	2.85	5.0	1.75	725	20.8	0.236	1.64			0.124	0.006	0.031
500	N_2	16	1062	14.99	1.4	4	56	15	4.90	4.2	0.86	825								
600	N_2	4	1064	14.98	1.5	7	67	5	17.38	4.0	0.23	775	21.7					0.119		
700	N_2	4	1073	14.99	1.3	7	66	7	12.29	4.0	0.33		13.2	0.276	0.76	0.53	0.49	0.174	0.003	0.019

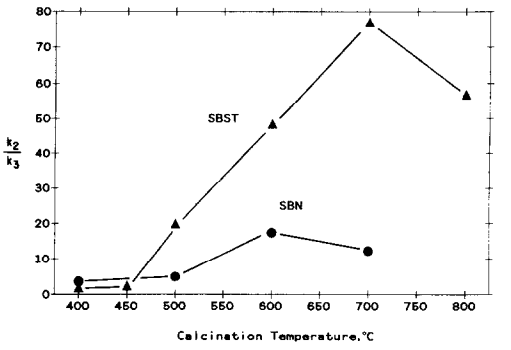

FIG. 4. DMA selectivity vs calcination temperature of shallow-bed and steamed H–RHO.

framework with half of the weight gain occurring in 9 min.

Figure 5 shows that DME yields are uniformly low (4–6%) as SBN T_c is increased from 400 to 700°C.

As shown in Fig. 6, increasing SBN T_c results in an increase in internal Lewis sites as measured by MeCN titration. Similar behavior is also noted in Fig. 7 for NH_4–RHO samples deammoniated *in situ* in the FTIR spectrometer. The increase in Lewis sites is accompanied by a corresponding decrease in Brønsted sites (3610 cm^{-1}). External Brønsted and Lewis sites decrease gradually over the range of T_c from 500 to 700°C (see Figs. 8 and 9).

C. *Shallow-Bed Steam Calcination*

In contrast to SBN calcination, SBST calcination of NH_4–RHO from T_c of 400 to

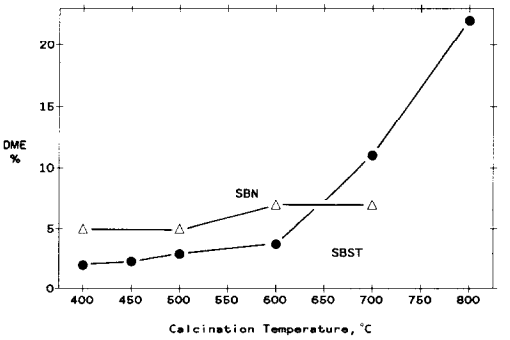

FIG. 5. DME yield vs calcination temperature of shallow-bed and steamed H–RHO.

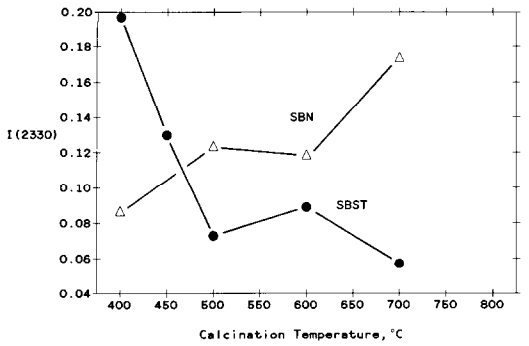

FIG. 6. Intensity of 2330 cm^{-1} MeCN band (internal Lewis sites) vs calcination temperature of shallow-bed and steamed H–RHO.

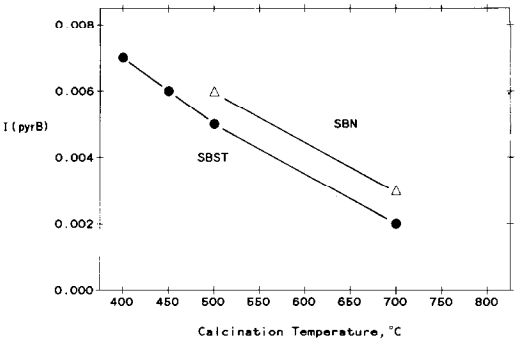

FIG. 8. Intensity of 1545 cm^{-1} pyridine band (external Brønsted sites) vs calcination temperature of shallow-bed and steamed H–RHO.

800°C leads to monotonically decreasing crystallinity (Fig. 2). SBST calcination results in greater levels of dealumination than SBN calcination as indicated in Fig. 3. The framework composition of H–RHO-SS873 is approximately $H_{5.3}Cs_{0.7}Al_6Si_{42}O_{96}$ (*19, 20*) after loss of ~5 framework Al atoms.

The SBST samples are characterized by a hydroxyl band at 3640 cm^{-1} (*19–21*). Ammonia desorption studies show that the acidity of the OH groups giving rise to this 3640 cm^{-1} band is substantially lower than the acidity of the 3610 cm^{-1} hydroxyls produced in SBN calcination (*19–21*). The intensity of the 3640 cm^{-1} band increases with T_c from 400 to 500°C and then decreases from 500 to 700°C (Fig. 10).

SBST calcination results in a large decrease in I(MeCN), Fig. 6, as T_c increases from 400 to 500°C. At $T_c > 500$°C the number of internal Lewis sites remains essentially constant. This is in contrast, however, to the SBN samples where the number of internal Lewis sites increases steadily with T_c.

Table 2 summarizes the physical and catalytic property data for a series of SBST H–RHO samples. In general the physical properties of SBST-calcined H–RHO change systematically with T_c: ν(TO) increases,

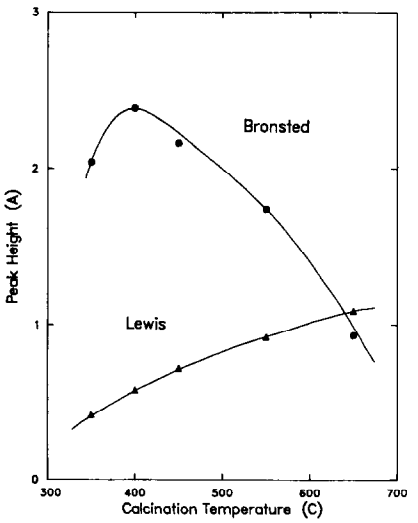

FIG. 7. Intensities of 2330 cm^{-1} MeCN band and 1545 cm^{-1} pyridine band vs *in situ* calcination temperature of NH_4–RHO.

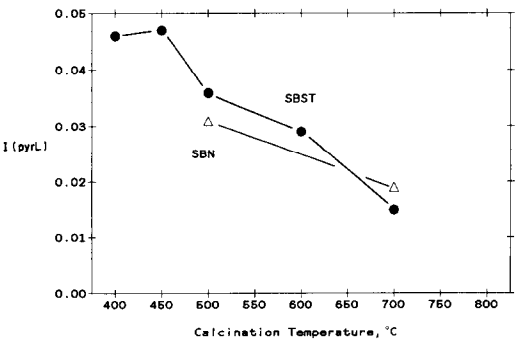

FIG. 9. Intensity of 1455 cm^{-1} pyridine band (external Lewis sites) vs calcination temperature of shallow-bed and steamed H–RHO.

TABLE 2

Effects of Calcination Temperature on Properties of Shallow-Bed Steamed and Deep-Bed Calcined H–RHO B (0.7 Cs/uc)

T (°C)	Atm[a]	Hour	ν(TO) (cm^{-1})	SV (h^{-1})	DME (%)	DMA (%)	TMA (%)	k_2/k_3	k_2	k_3	I_{max} (cps)	MeOH (%)	I(OH) (3740 cm^{-1})	I(OH) (3610 cm^{-1})	I(OH) (3640 cm^{-1})	I(OH) (3680 cm^{-1})	I(MeCN) (2330 cm^{-1})	I(PyrB) (1545 cm^{-1})	I(PyrL) (1455 cm^{-1})
400	H_2O/N_2	4	1065	5.3	2.0	45	25	1.93	3.4	1.75	1340	23.7	0.140	1.76	0.6SH[b]		0.197	0.007	0.046
450	H_2O/N_2	4	1068	5.3	2.3	52	20	2.45	3.0	1.22	1067	24.2	0.160	1.64	1.2SH		0.130	0.006	0.047
500	H_2O/N_2	4	1071	5.0	2.9	69	6	20.00	3.3	0.17	1089	22.8	0.236	None	1.29S[c]	None	0.073	0.005	0.036
600	H_2O/N_2	4	1073	3.3	3.7	69	2	48.50	3.2	0.07	676		0.315		0.69	0.2SH	0.089	0.008	0.029
700	H_2O/N_2	4	1085	1.3	11.0	71	1	77.00	6.5	0.08	529	17.6	0.575		0.52	0.4	0.057	0.002	0.015
800	H_2O/N_2	4	1090	0.3	22.0	70	4	57.00	10.9	0.19	228	13.6							
650	Air/DB	4	1071	6.7	4.2	51	15	3.50	3.4	0.97	960		0.240	1.10	1.20		0.140	0.006	0.026

[a] $p(H_2O)$ = 612 Torr.
[b] SH, shoulder.
[c] S, saturated spectra.

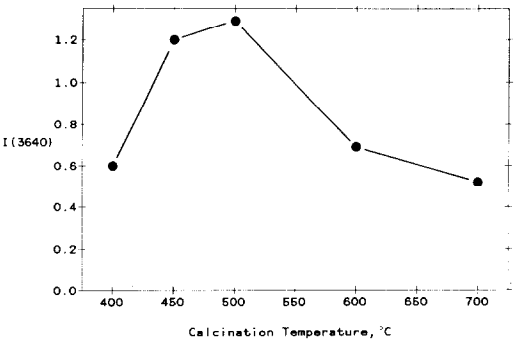

FIG. 10. Intensity of 3640 cm^{-1} OH band vs calcination temperature of steamed H–RHO.

terminal OH concentration (3740 cm^{-1}) increases, and the number of internal and external Lewis and Brønsted sites decreases (Figs. 6–9, 11). Samples calcined at 400 and 450°C are not completely deammoniated as evidenced by a residual NH_4^+ IR band at 1450 cm^{-1}. Catalytic activity remains high for T_c = 400–500°C and declines significantly as T_c increases from 500 to 700°C and then levels off (Fig. 12). The low DMA selectivities at T_c = 400 and 450°C are attributed to incomplete deammoniation (Fig. 4). Steaming clearly produces higher DMA selectivity and lower TMA selectivity than SBN calcination. SBST calcination also reduces DME yield more than SBN calcination as shown in Fig. 5. As T_c is increased beyond 600°C, the DME yield increases substantially.

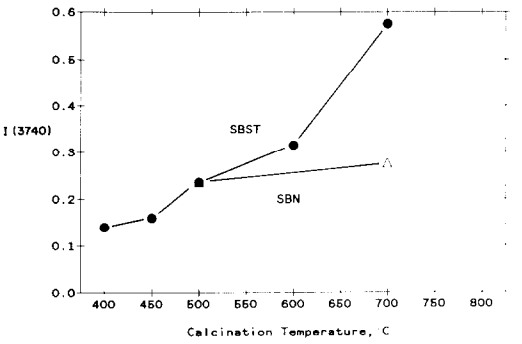

FIG. 11. Intensity of 3740 cm^{-1} OH band vs calcination temperature of shallow-bed and steamed H–RHO.

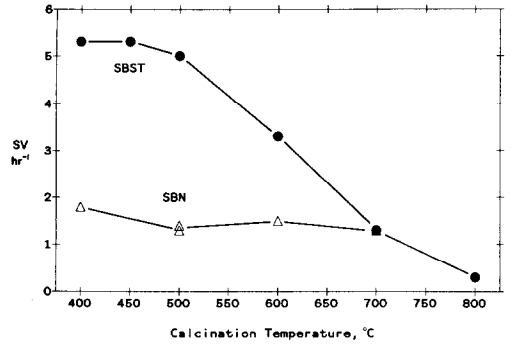

FIG. 12. Catalytic activity vs calcination temperature of shallow-bed and steamed H–RHO.

Catalytic and physical properties were determined for samples of H–RHO calcined at 600°C where steam partial pressure was varied from 0.6 to 612 Torr (Table 3). As shown in Fig. 13, k_2/k_3, the rate of formation of DMA relative to TMA formation, depends strongly on $p(H_2O)$.

Increasing steam pressures during calcination results in progressively greater intensities of the 3740 cm^{-1} terminal OH and ν(TO) stretching bands (Figs. 14 and 15). The effects are somewhat greater for steaming of H–RHO than for steaming of NH_4–RHO. This probably occurs because of previous framework damage involved in preparing H–RHO. The intensity of the 3640 cm^{-1} band also increases with $p(H_2O)$ but much more rapidly than ν(TO) or the 3740 cm^{-1} band. The maximum intensity of the 3640 cm^{-1} band is attained at 100 Torr

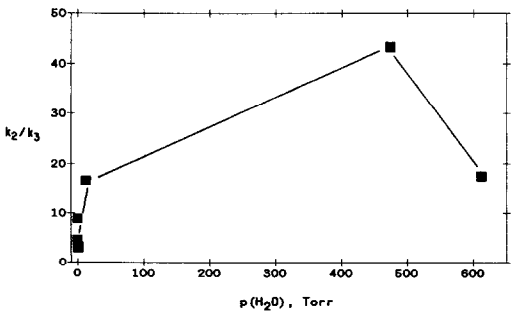

FIG. 13. DMA selectivity (k_2/k_3) of steamed H–RHO vs steam partial pressure ($p(H_2O)$).

TABLE 3

Effects of Steam Pressure on Properties of H–RHO B Calcined at 600°C

Treatment	$p(H_2O)$ (Torr)	ν(TO) (cm^{-1})	SV (h^{-1})	DME (%)	DMA (%)	TMA (%)	k_2/k_3	k_2	k_3	MeOH (%)	I(OH) (3740 cm^{-1})	I(OH) (3610 cm^{-1})	I(OH) (3640 cm^{-1})	I(OH) (3680 cm^{-1})	I(MeCN) (2330 cm^{-1})	I(PyrB) (1545 cm^{-1})	I(PyrL) (1455 cm^{-1})
$N_2 + H_2O/N_2$ SB	612.0	1074	2.9	5.8	69	4	17.52	4.4	0.25	19	0.423	None	2.0S	0.4SH	0.079	0.002	0.019
$N_2 + H_2O/N_2$ SB	474.0	1073	3.8	4.5	69	2	43.30	3.2	0.07		0.189	None	1.75S	0.2SH	0.048	0.000	0.018
$N_2 + H_2O/N_2$ SB	108.0	1071									0.244	None	2.13S	None	0.086	0.003	0.023
$N_2 + H_2O/N_2$ SB	12.4	1070	5.3	1.8	67	5	16.60	3.5	0.21		0.230	None	1.39S	None	0.142	0.004	0.040
$N_2 + H_2O/N_2$ SB	1.2	1066	3.7	4.4	58	14	3.15	2.8	0.89		0.210	1.78S	1.1SH		0.182	0.006	0.057
$N_2 + H_2O/N_2$ SB	0.6	1067	3.7	5.7	55	13	2.93	2.5	0.85		0.160	1.18	0.6SH		0.154	0.005	0.037
N_2 SB	0.0		6.7	4.1	57	20	4.52	5.2	1.15	22	0.172	0.79			0.174	0.008	0.032
N_2 SB	0.0	1060	2.1	8.8	67	11	8.88	5.7	0.64		0.219	1.63	0.1SH		0.226	0.006	0.033

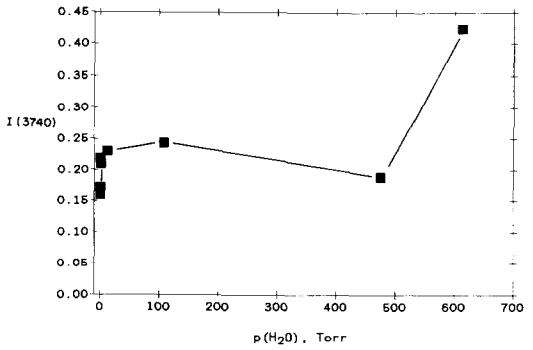

FIG. 14. Intensity of 3740 cm^{-1} OH band in steamed H–RHO vs steam partial pressure ($p(H_2O)$).

for both H–RHO and NH_4–RHO. The 3640 cm^{-1} band seems to develop at somewhat lower $p(H_2O)$ for H–RHO than for NH_4–RHO.

Increases in T_c and $p(H_2O)$ during SBST calcination cause decreases in acid site populations (internal Lewis, external Lewis, and Brønsted sites) which parallel the increases in k_2/k_3, ν(TO), 3740 and 3640 cm^{-1} bands in H–RHO.

D. Deep-Bed Calcination

Deep-bed calcination conditions were not explored in detail because this process produces catalysts with properties intermediate between the SBN and SBST samples and generally lower DMA selectivities. The properties of a DB-calcined H–RHO are listed in Table 2. A typical DB-calcined H–RHO was described by Fischer *et al.* (*12*).

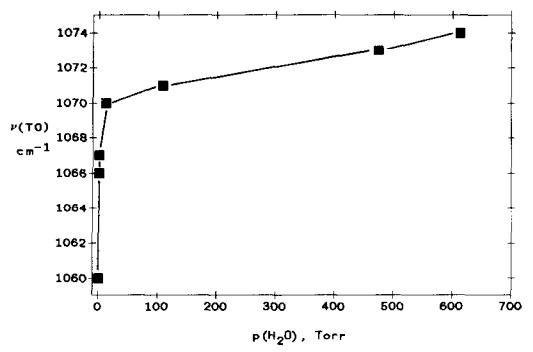

FIG. 15. TO stretching frequency (ν(TO)) of steamed H–RHO vs steam partial pressure ($p(H_2O)$).

Significant dealumination is evident from the elevated ν(TO) = 1071 cm^{-1}. The higher crystallinity relative to SBN results from the steam partial pressure generated in the closed container. The IR absorption spectrum indicates that about half of the 3610 cm^{-1} hydroxyls have been converted to 3640 cm^{-1} hydroxyls. The catalytic properties of H–RHO-D923 are similar to those of a SBST sample calcined at 450–500°C.

E. Reproducibility

As mentioned earlier, typical RHO preparations are not free of impurities. Because these impurities have different methylamine selectivities, a certain degree of variability is anticipated from different RHO preparations. Tables 4A and 4B summarize the properties of H–RHO samples obtained from six different NH_4–RHO precursors and allow comparison of SBN and SBST treatment of samples of H–RHO from the same preparation. Five samples have "normal" purity levels but one (sample F) has an unusually large amount of P_c and pollucite. Mean crystallite size of all samples varied from 0.4 to 0.6 μm. The H–RHO catalysts were prepared by SBN calcination at 600°C for 4 h (Table 4A) or by SBST calcination of H–RHO at 600°C for 4 h (Table 4B). The approximate purity of these RHOs was established using MeOH sorption data. The five "normal" samples absorb 21.5–23.0% MeOH compared to a hypothetical value of 24.0% for a pure sample with Cs/uc = 1. The sample containing P_c and pollucite sorbs only 19.1% MeOH. The Cs content variation arises from differing degrees of NH_4^+ exchange. These variations in Cs content do not influence the catalytic properties (*22*).

The DMA selectivities of the SBN samples show a wide variation from 46 to 65% with a mean value of 57%. Sample A has unusually high DMA selectivity and rather high 3740 cm^{-1} OH band intensity but is otherwise indistinguishable from samples B–D of normal purity. Sample F with measurable quantities of P_c and pollucite has

TABLE 4A

Properties of Six Different RHO Preparations Shallow-Bed Dry Calcined at 600°C

Source	Cs/uc	ν(TO) (cm^{-1})	SV (h^{-1})	DME (%)	DMA (%)	TMA (%)	k_2/k_3	k_2	k_3	MeOH (%)	I(OH) (3740 cm^{-1})	I(OH) (3610 cm^{-1})	I(OH) (3640 cm^{-1})	I(OH) (3680 cm^{-1})	I(MeCN) (2330 cm^{-1})	I(PyrB) (1545 cm^{-1})	I(PyrL) (1455 cm^{-1})
RHO-A	1.00	1062	2.2	5.5	65	9	10.58	4.6	0.43	21.8	0.323	0.880	NV[a]		0.203	0.007	0.027
RHO-B	0.70	1061	6.7	4.1	57	20	4.52	5.2	1.15	22.0	0.172	0.790	NV		0.174	0.008	0.032
RHO-C	0.25	1063	2.5	15.0	56	19	4.50	4.7	1.05	23.3	0.186	0.904	NV		0.245	0.005	0.030
RHO-D	0.70		2.0	13.0	53	15	4.21	4.0	0.96	21.5	0.189	0.998	NV		0.220	0.011	0.037
RHO-E	0.50		0.8	9.0	64	8	39.00	4.0	0.10	20.6	0.142	1.500	NV		0.196	0.004	0.028
RHO-F	0.60	1063	1.8	16.0	46	21	2.50	3.9	1.60	19.1	0.170	0.791	NV		0.169	0.005	0.026
Mean values		⟨1062⟩	⟨2.7⟩	⟨10.7⟩	⟨57⟩	⟨15⟩	⟨5.2⟩	⟨4.4⟩	⟨1.04⟩		⟨0.20⟩				⟨0.201⟩	⟨0.007⟩	⟨0.030⟩

[a] Not visible.

TABLE 4B

Properties of Six Different RHO Preparations Shallow-Bed Steamed at 600°C

Source	Cs/uc	ν(TO) (cm^{-1})	SV (h^{-1})	DME (%)	DMA (%)	TMA (%)	k_2/k_3	k_2	k_3	MeOH (%)	I(OH) (3740 cm^{-1})	I(OH) (3610 cm^{-1})	I(OH) (3640 cm^{-1})	I(OH) (3680 cm^{-1})	I(MeCN) (2330 cm^{-1})	I(PyrB) (1545 cm^{-1})	I(PyrL) (1455 cm^{-1})
RHO-A	1.00	1074	3.2	4.3	64	10	8.2	4.4	0.53		0.260	None	0.9S[a]	0.4SH[b]	0.106	0.002	0.031
RHO-B	0.70	1072	3.2	3.1	61	10	6.9	2.6	0.37		0.254	None	2.0S		0.073	0.002	0.023
RHO-C	0.25	1073	3.2	2.6	66	7	10.0	3.0	0.30		0.291	None	2.1S		0.106	0.003	0.030
RHO-D	0.70	1076	3.2	3.0	62	6	8.8	2.8	0.32	19.8	0.236	None	1.6S		0.098	0.002	0.030
RHO-E	0.50	1073	4.0	4.1	64	7	7.6	2.5	0.32		0.213	None	1.7S		0.066	0.002	0.025
RHO-F	0.60	1073	3.3	3.5	62	6	10.3	3.5	0.37	18.7	0.232	None	1.3S		0.085	0.008	0.022
Mean values		⟨1073⟩	⟨3.4⟩	⟨3.3⟩	⟨63⟩	⟨8⟩	⟨8.8⟩	⟨3.3⟩	⟨0.38⟩		⟨0.255⟩				⟨0.094⟩	⟨0.003⟩	⟨0.027⟩

[a] S, saturated spectra.
[b] SH, shoulder.

significantly lower DMA selectivity and lower activity than the purer samples. The considerable variation in DME yield as well as the unusually high activity of sample B does not correlate with other observed quantities.

The SBST samples show an increased degree of dealumination and framework damage compared to the SBN calcinations: $\langle \nu(\text{TO}) \rangle = 1062 \rightarrow 1073$ cm^{-1} and $\langle I(3740) \rangle = 0.20 \rightarrow 0.25$. Similar changes can also be seen in the number of internal Lewis sites where $I(\text{MeCN}) = 0.201$ (SBN) $\rightarrow 0.089$ (SBST) and external Brønsted sites where $I(\text{PyrB}) = 0.007 \rightarrow 0.003$. Sample F with the high impurity content has an exceptionally high value of $I(\text{PyrB}) = 0.008$ after steam calcination. However, the number of external Lewis sites is not substantially affected by the calcination atmosphere, SBN vs SBST.

The activities of the SBN samples show a wide variation whereas, after steam treatment, activities are quite similar. Furthermore, after SBST calcination at 600°C these samples attain uniformly high DMA selectivity ($\langle \text{DMA} \rangle = 63.1 \pm 2\%$). Sample F, which contained large quantities of P_c and pollucite, was indistinguishable in catalytic behavior from the "normal" samples of H–RHO after steaming.

DISCUSSION

A. Effects of T_c on Physical Properties

As T_c is increased, X-ray crystallinity (Fig. 2) decreases gradually for SBST samples while remaining nearly constant for SBN samples. An increase in T_c also causes loss in intensity of the 3610 cm^{-1} OH band and increases in the TO stretching frequency and the intensity of the terminal OH stretching band at 3740 cm^{-1}. These changes reflect framework dealumination which is believed to lead to framework damage and/or loss of crystallinity. In the case of SBN samples, the absence of H_2O is believed to prevent Si mobility and probably leads to more crystalline defects and to an earlier collapse of the crystal structure. Dealumination presumably occurs to a greater degree in steamed samples because of increased mobility of $Al(OH)_x$ and $Si(OH)_x$ species in steam. There may be more Si replacement of Al in a steam atmosphere. Several possibilities for the source(s) of these SiOH groups include (i) amorphous $Al_2O_3 \cdot 6SiO_2$ created from the destruction of RHO, chabazite, and/or P_c phases; (ii) SiO_2 clusters in pores created by Si migration from crystalline regions to Al vacancies or by formation of SiOH groups at the pore walls; and (iii) the presence of SiOH groups at the external surface of the RHO crystallites due to Si migration.

In contrast to SBN calcination, calcination under SBST and DB conditions produces IR OH bands at 3640 cm^{-1} (Fig. 10). Under SBST conditions this band, which arises from weakly acidic OH groups, is very strong and sharp. Acidity was evaluated by (i) H NMR where the H chemical shift has been shown to be 2.1 ppm (*21*) and (ii) an IR study where NH_3 was found to desorb at low temperatures from these sites (*19–21*). Structural studies based on neutron powder diffraction data (*20*) indicate that this is a bridging OH and that the frequency shift from 3610 cm^{-1} is probably caused by the proximity of nonframework Al (NFA) species to the OH.

At $T_c > 500$°C the 3640 cm^{-1} band declines and another OH band appears at 3680 cm^{-1}. This band is believed to result from condensed Al–O species, perhaps a boehmite-like AlOOH cluster (*23*).

The number of internal Lewis sites increases slightly with increasing T_c under SBN conditions. This increase may be related to the appearance of NFA species (*18*) or perhaps to the formation of Al vacancies under shallow-bed conditions where migration of $Si(OH)_x$ species to replace Al vacancies is minimized.

Under steaming conditions migration of about one-half of the framework Al atoms seems to be associated with reduced Brønsted acidity (*19*). Al vacancies are

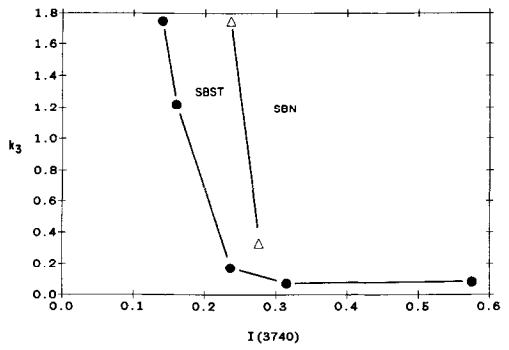

FIG. 16. TMA selectivity of shallow-bed and steamed H–RHO vs intensity of 3740 cm^{-1} OH band.

healed by migrating $Si(OH)_x$. The number of Lewis sites decreases gradually through the temperature range 400–700°C (Table 2). This reduction may occur as the result of the migration of Al atoms to the vicinity of OH groups or of the formation of neutral NFA species such as Al_2O_3 or $[AlO^+ + AlO_2^-]$ (*19–21*).

The decreases in external Lewis and Brønsted sites with increased T_c are probably caused by amorphitization of the impurities chabazite, pollucite, and P_c as well as from the deactivation of the external surface of H–RHO (*24*). Dependence of the MeCN, PyrL, and PyrB bands on T_c of the impurity phases was not determined.

B. Catalytic Studies

1. Selectivity. Because DMA is smaller than TMA and we know that TMA can be sorbed into H–RHO SBN and H–RHO SBST, we believe that TMA diffusivity is smaller than that of DMA. By analogy with size and shape selectivity studies in ZSM-5, it seems possible that DMA selectivity in H–RHO could arise from hindered TMA diffusion. In this part of the discussion, hindered TMA diffusivity will be related to changes shown by H–RHO during calcination.

The rate constant for TMA synthesis, k_3, decreases while the frequency of the TO stretching band and the intensity of the 3740 cm^{-1} OH band (Figs. 16 and 17) increase for both SBN and SBST samples. In addition, the rate of DMA formation, k_2, is nearly constant. This suggests that the reduced TMA selectivity is related to the dealumination process.

There is also a strong correlation between k_3 and the number of external acid sites as determined by pyridine titration (Tables 1 and 2). This suggests that the external surfaces of either impurity phases (chabazite, P_c, or pollucite) or the RHO zeolite itself are nonselective toward DMA but do contribute to the overall product distribution.

The development of the 3640 cm^{-1} band does not parallel TMA formation. Therefore, although the structural feature responsible for this band seems to be associated with low TMA production, only small numbers of this species, if any at all, are necessary for good selectivity toward DMA.

Development of improved DMA selectivity is activated by the effects of time and temperature. This process could conceivably be the amorphitization and deactivation of the impurity phases and/or dealumination. If hindered TMA diffusivity is the predominant mechanism, high DMA selectivity could result from the formation of nonframework Al species. Extraction of Al from the framework results in Al_xO_y species which, either by themselves or after adsorption of an amine at an Al_xO_y or the vacancy created upon dealumination, have

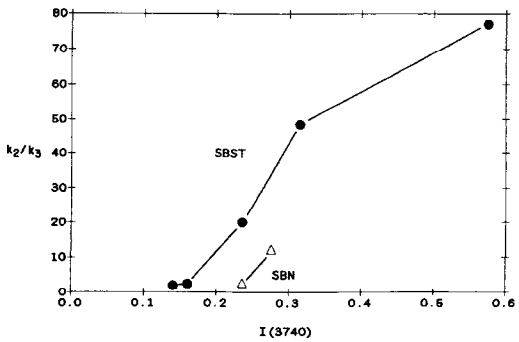

FIG. 17. DMA selectivity of shallow-bed and steamed H–RHO vs intensity of 3740 cm^{-1} OH band.

the potential of being located in either the six-rings or the eight-rings and serving as barriers for TMA diffusion. Although the evidence for dealumination and the formation for the of NFA species in SBN H–RHO and SBST H–RHO is strong, the nature and location of these species is not well established. The best knowledge we have now is for an AlO^+ group in the six-ring and the presence of a neutral Al_xO_y group in SBST H–RHO. Nonframework Al species in the six-ring would not hinder TMA diffusion but there are other potential sources of reduced TMA diffusivity:

- The AlO^+ ion is part of an Al_2O_3 molecule where the remainder of the molecule could extend into the eight-ring and provide the required barrier.
- The remaining atoms, AlO_2^-, are located in the eight-ring, again providing the required barrier to TMA diffusion.
- NH_3 and/or methylamines are strongly adsorbed on the AlO^+ or Al_2O_3 molecule.

Unfortunately, we have only indirect evidence for these possibilities. NMR studies confirm the framework dealumination, show that the protons are not very acidic, and indicate the presence of octahedral Al and distorted tetrahedral Al (many more in SBN H–RHO than in SBST H–RHO), but do not provide us with direct evidence for the nature of the NFA species.

The situation with SBN H–RHO is somewhat different in that there are fewer NFA species and it is not known whether they are cationic or neutral. These species are less likely to be mobile during their formation and may also be associated with Al or O vacancies. The same possibilities for the NFA species alone or as an NFA/NH_3 or an NFA/methylamine adsorption complex exist for the SBN samples.

The correlation between TMA selectivity and numbers of external acid sites suggests that nonselective P_c and pollucite and less selective chabazite, the most common impurities, contribute significantly to the product distribution when calcined below 500°C and that calcination at increasingly higher temperatures progressively deactivates these constituents.

Mechanisms for DMA selectivity enhancement involving NFA generation and impurity deactivation may both operate under most calcination conditions.

2. Activity. The high methylamine activities obtained on SBN-calcined RHO are improved even further by SBST calcination of RHO. Changes that occur on steaming that might lead to higher activity over SBST samples are destruction of the external surface of impurity phases, reduction of internal Lewis sites, higher crystallinity at $T_c <$ 600°C, and destruction of the 3610 cm^{-1} OH groups with replacement by 3640 cm^{-1} OH groups.

Although steaming destroys the external surface of impurity phases and the Lewis sites associated with these impurities (*24*), these changes are probably not responsible for the increased activity of steamed samples. Deactivation of a 5–10% impurity fraction would dilute the active material and reduce the activity.

Although increased crystallinity for calcination temperatures of 500°C might lead to increased activity, this would not explain the better activity of SBST samples with T_c = 600°C where crystallinities of SBN and SBST samples are similar.

A more likely explanation of the higher activity of SBST samples is as follows. Good methylamine activities are obtained from SBN-calcined samples and even higher activities from SBST samples. The SBN samples contain primarily strongly acidic 3610 cm^{-1} Brønsted sites and only a few Lewis sites whereas the SBST samples contain no apparent 3610 cm^{-1} sites but a small number of strong acid sites of unknown type and many weak acid sites originating from bridging OH groups (3640 cm^{-1}) (*13, 19–21*). The majority of the 3610 cm^{-1} sites in the SBN samples must contribute little to the activity; their replacement in SBST samples by primarily 3640 cm^{-1} sites and the small number of strong

acid sites of unknown origin must be responsible for the increased activity. It is possible that the weaker acid sites in the SBST catalysts desorb MMA, DMA, and TMA more readily, thus facilitating MeOH adsorption and promoting the methanol–ammonia reaction.

The concept of only a small number of active sites necessary for efficient zeolite catalytic activity is not novel. In general it has been concluded that acid-catalyzed reactions over zeolites depend on the presence of Brønsted sites (*25*), that the maximum activity occurs with many Lewis sites present, and that only very few, presumably very strong OH sites are active. The activity of many reactions over zeolites has been shown to reach a maximum where most of the Brønsted acid sites have been destroyed and many Lewis acid sites form (presumably from NFA species): alkylation of benzene over H–Y activated at 600°C (*26*); disproportionation of toluene over H–Y and H–mordenite calcined at 575 and 700°C, respectively (*27*); NO adsorption on H–Y calcined at 600°C (*28*); redox activity using tetracyanoethylene and perylene on H–Y calcined at T = 600–660°C (*29, 30*); SO_2^- radical formation from SO_2 exposure on HY calcined at 600°C (*31*); and cumene cracking over H–Y calcined at 650°C (32). Jacobs *et al.* studied cumene cracking and toluene disproportionation and concluded that although OH groups were the active sites for the reactions, only a small fraction of the total OH groups are active sites, specifically the very strong acid sites. They also concluded, along with Lunsford (*28*), that the effectiveness of Brønsted sites may be enhanced by the development of sites (NFA) created during the dehydroxylation process.

We have no evidence for whether the active sites in H–RHO are Brønsted or Lewis acid sites, but it has been stated that Lewis sites are not effective in catalyzing the methylamine reactions (*11*). Our catalytic data over γ-Al_2O_3, a catalyst containing only Lewis sites, support this view. It

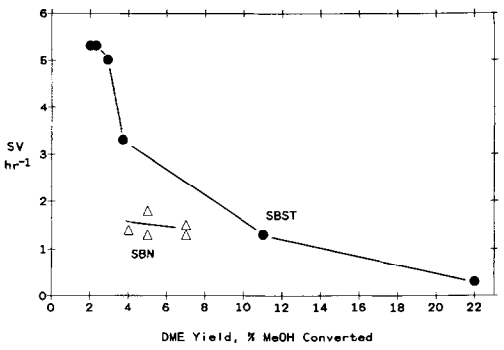

FIG. 18. Catalytic activity of shallow-bed and steamed H–RHO vs DME yield.

shows only moderate activity at 325°C (SV= 0.1–0.2) and is TMA selective (k_2/k_3 = 0.6). The methylamine reaction over H–RHO is probably similar to the other reactions described above. The lower activity of the SBN samples would then arise because of the strong adsorption of NH_3 and methylamines and relative exclusion of MeOH from the large number of strong Brønsted sites.

The sudden decrease in activity of samples steamed at $T_c > 700$°C is accompanied by concomitant changes in ν(TO) from 1062 to 1074 cm^{-1} (Table 2) and in DME yield to a value >20% (Figs. 18 and 19). We propose that this decrease in activity results from both loss of zeolite crystallinity (see Fig. 20) and formation of boehmite-like clusters.

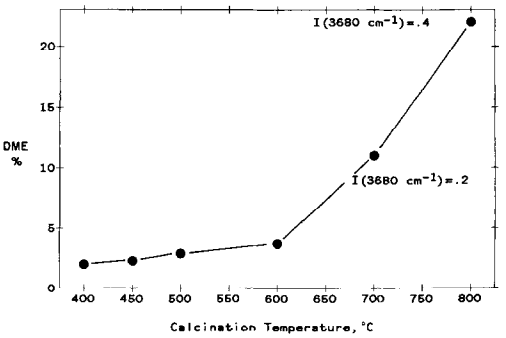

FIG. 19. DME yield of steamed H–RHO vs calcination temperature.

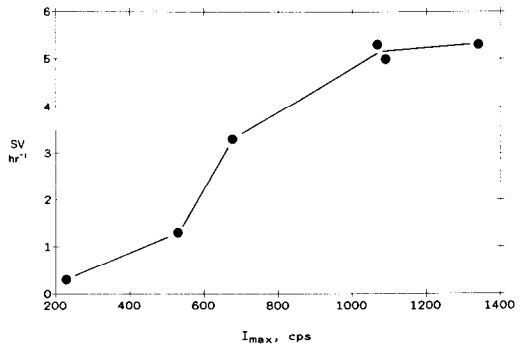

FIG. 20. Catalytic activity of steamed H–RHO vs intensity of RHO 420 peak (X-ray crystallinity).

C. DME Yield

Decreased activity over samples calcined at T_c = 700 and 800°C (Fig. 12 and Table 2) is marked by increased DME yields (Figs. 5 and 19). Condensed NFA species could be responsible for the increased DME yields. Support for this hypothesis comes from the observation of the growth of the 3680 cm^{-1} band with T_c > 700°C (Fig. 19). As noted earlier, the 3680 cm^{-1} band is believed to result from condensed Al–O species. The condensation could result in destruction of some acidic sites, while creating new sites (3680 cm^{-1}). The catalytic dehydration of MeOH to DME over alumina catalysts is well known.

CONCLUSIONS

Selectivity and activity of zeolite H–RHO in the reaction of methanol and ammonia to methylamines are highly dependent upon the temperature and atmosphere of calcination of NH_4–RHO and the nature and amount of impurities present. DMA selectivity increases with temperature of calcination and with steaming. Changes in physical properties that accompany these increases in DMA selectivity are increased dealumination and decreases in external Lewis and Brønsted sites. These changes suggest that the increased DMA selectivity results from decreased TMA diffusivity and/or destruction of TMA selective impurities such as pollucite. Decreased TMA diffusivity could arise from the presence of nonframework Al species in or near the eight-ring windows, either alone or as an adsorption complex formed from the NFA and the methylamines.

Increased DME yield in samples calcined above 600°C occurs because of nonframework Al condensation.

Activities of *steamed* SB samples are higher than those of *dry* SB Samples. This correlates with the destruction of most of the highly acidic 3610 cm^{-1} Brønsted sites and to the formation of many weakly acidic 3640 cm^{-1} OH sites. We hypothesize that the catalytic activity of both steamed and dry SB-calcined H–RHO is due to a small number of highly acidic sites. Removal of the majority of the 3610 cm^{-1} OHs and substitution of the weaker 3640 cm^{-1} OHs allow weaker adsorption of methylamines, more facile adsorption of MeOH, and, therefore, a more efficient reaction of MeOH with NH_3 and amines. Decreased activity of the SBST samples with increasing T_c results from framework damage.

ACKNOWLEDGMENTS

We thank C. Foris and R. Harlow for assistance with the X-ray diffraction data, M. Van Kavelaar for the SEM photographs, E. Matthews for determining the TO stretching frequencies, and W. Farneth for valuable discussions.

REFERENCES

1. Keane, W., Sonnichsen, G. C., Abrams, L., Corbin, D. R., Gier, T. E., and Shannon, R. D., *Appl. Catal.* **32,** 361 (1987).
2. Gier, T. E., Shannon, R. D., and Sonnichsen, G. C., U.S. Patent 4,602,112 (July 22, 1986).
3. Abrams, L., Gier, T. E., Shannon, R. D., and Sonnichsen, G. C., Eur. Patent Applic. 183,423 (April 6, 1986).
4. Cochran, R. N., and Deeba, M., U.S. Patent 4,398,041 (August 9, 1983).
5. Deeba, M., Ambs, W. J., and Cochran, R. N., U.S. Patent 4,434,300 (February 28, 1984).
6. Tompsett, A. J., U.S. Patent 4,436,938 (March 13, 1984).
7. Parker, D. G., and Tompsett, A. J., G.B. Patent 2019394B (September 2, 1982).
8. Tompsett, A. J., and Whittam, T. V., Eur. Patent Applic. 107,457 (February 5, 1984).

9. Ashina, Y., Fujita, T., Fukatsu, M., and Yagi, J., Eur. Patent Applic. 125,616 (November 21, 1984).
10. Ashina, Y., Fujita, T., Fukatsu, M., and Yagi, J., Eur. Patent Applic. 130,407 (September 1, 1985).
11. Mochida, I., Yasutake, A., Fujitsu, H., and Takeshita, K., *J. Catal.* **82,** 313 (1983).
12. Fischer, R. X., Baur, W. H., Shannon, R. D. Staley, R. H., Vega, A. J., Abrams, L., and Prince, E., *J. Phys. Chem.* **90,** 4414 (1986).
13. Shannon, R. D., Staley, R. H., and Auroux, A., *Zeolites* **7,** 301 (1987).
14. Stabler, R. N., and Chesnick, J., *Intl. J. Chem. Kinet.* **10,** 461 (1978).
15. Barrer, R. M.,. Baynham, J., Bultitude, F. W., and Meier, W. M., *J. Chem. Soc.,* 195 (1959).
16. Barrer, R. M., Bultitude, F. W., and Kerr, I. S., *J. Chem. Soc.,* 1521 (1959).
17. Taylor, A. M., and Roy, R., *Amer. Mineral.* **49,** 656 (1964).
18. Baur, W. H., Fischer, R. X., Shannon, R. D., Staley, R. H., Vega, A. J., Abrams, L., Corbin, D. R., and Jorgensen, J. D., *Z. Kristallogr.* **179,** 281 (1987).
19. Fischer, R. X., Baur, W. H., Shannon, R. D., and Staley, R. H., *J. Phys. Chem.* **91,** 2227 (1987).
20. Fischer, R. X., Baur, W. H., Shannon, R. D., Staley, R. H., Abrams, L., Vega, A. J., and Jorgensen, J. D., *Acta Crystallogr.,* in press.
21. Shannon, R. D., Staley, R. H., Vega, A. J., Fischer, R. X., Bauer, W. H., and Auroux, A., to be published.
22. Keane, M., and Shannon, R. D., unpublished results.
23. Shannon, R. D., Gardner, K. H., Staley, R. H., Bergeret, G., Gallezot, P., and Auroux, A., *J. Phys. Chem.* **89,** 4778 (1985).
24. Shannon, R. D., Keane, M., Abrams, L., Staley, R. H., Gier, T. E., Corbin, D. R., and Sonnichsen, G. C., *J. Catal.,* in press.
25. Bartomeuf, D., "Zeolites: Science and Technology NATO Adv. Study Inst. on Zeolites Alcabideche, Portugal, 1984," pp. 317–346.
26. Venuto, P. B., Hamilton, L. A., Landis, P. S., and Wise, J. J., *J. Catal.* **4,** 81 (1966).
27. Benesi, H., *J. Catal.* **8,** 368 (1967).
28. Lunsford, J. H., *J. Phys. Chem.* **72,** 4163 (1968).
29. Flockhart, B. D., McLoughlin, L., and Pink, R. C., *J. Catal.* **25,** 305 (1972).
30. Flockhart, B. D., Megarry, M. C., and Pink, R. C., "Molecular Sieves," Adv. in Chem., Ser. 121. Amer. Chem. Soc., Washington, DC, 1973.
31. Ono, Y., Tokunaga, H., and Kell, T., *J. Phys. Chem.* **79,** 752 (1975).
32. Jacobs, P. A., Leeman, H. E. and Uytterhoeven, J. B., *J. Catal.* **33,** 17, 31 (1974).